We are IntechOpen,
the world's leading publisher of
Open Access books
Built by scientists, for scientists

6,900
Open access books available

186,000
International authors and editors

200M
Downloads

Our authors are among the

154
Countries delivered to

TOP 1%
most cited scientists

12.2%
Contributors from top 500 universities

CLARIVATE ANALYTICS
BOOK CITATION INDEX
INDEXED

WEB OF SCIENCE™

Selection of our books indexed in the Book Citation Index
in Web of Science™ Core Collection (BKCI)

Interested in publishing with us?
Contact book.department@intechopen.com

Equivalent Nanocircuit Theory and Its Applications

Qing Zhang, Jun You and Chengpu Liu

Additional information is available at the end of the chapter

Abstract

A new methodology termed as equivalent nanocircuit (EN) theory is briefly introduced, and its recent important progress in designing meta-material devices with peculiar characteristics in optical or infrared frequency domain is reviewed. Three representative EN-based designs of infrared window meta-materials, such as Butterworth filter, metal-insulator-metal absorber and design-simplified TCO-based super-flat absorber, are demonstrated. All these progresses clearly indicate that the EN theory provides an inspiring advancement on the way of designing more complicated meta-devices.

Keywords: meta-material, metatronics, nanocircuit theory, surface plasmon polariton

1. Introduction

The functionalities of plasmonic nanodevices are dependent on their artificial structure parameters that usually are smartly engineered. To introduce convenient and feasible methods based on new paradigms to guide, the structure design is eagerly demanded. In the radio or microwave frequency domains, lumped circuit elements, e.g. resistors (R), inductors (L) and capacitors (C), can be effectively and flexibly used as blocks for designing complicated micro-electronic devices, and the conventional circuit theory is widely and successfully adopted. One question naturally arises: can such a circuit theory, along with its accompanying mathematical machinery, be extended and applied to the design of plasmonic nanostructures working at the optical domain?

Within this context, in this chapter, a new methodology, 'equivalent nanocircuit (EN) theory' is briefly introduced, and its representative applications in designing plasmonic devices with peculiar characteristics in optical or infrared frequency domains are enumerated. First, to start with the short introduction of the basis of 'metatronics', the analogy between micro-electronic lumped circuit elements (R, L, C) and optical nanocircuit elements (nanoparticles, nano-antennas, nanogratings and optical meta-surfaces) is established. Second, the method describing

how to use the above optical nanocircuit elements to construct a single-layer or multiple-layer complicated meta-material structure is proposed and thus the 'metatronics' concept moves forward to the multi-order circuit theory. Finally, three representative applications of multi-order EN theory to design infrared window meta-materials are demonstrated: (1) a synthesis procedure for designing a third-order Butterworth filter is proposed; (2) a metal-insulator-metal (MIM) ultra-broadband absorber is successfully designed in the infrared range; (3) with the transparent conductive oxides (TCOs) semiconductor materials as building blocks, a design-simplified broadband super-flat perfect infrared absorber is realized.

2. Metatronics and optical nanocircuit

2.1. 'Metatronics': meta-material-inspired optical circuitry

Optical meta-material bridges the gap between the conventional optics and the nanoworld, which gives rise to a diversity of surprising and profound effects fully appreciated and techno-logically explored in recent years [1–3]. The electromagnetic property of meta-materials is dependent on their specifically and smartly engineered artificial structures. To explore new design methodology is eagerly demanded. Historically, in electronics, basic functionalities are synthesized by 'lumped' circuit elements, such as resistors, inductors, capacitors and transistors, and more complicated operations can be realized by combining them into a complicated circuit in some specific serial or parallel ways. Now, great interests in pushing classic circuit operation to infrared or visible optical frequency range have boomed in order to achieve an optical analogy [4–7]. Generally, just simply reducing the basic unit size of circuit to the micrometre (μm) or nanometre (nm) level would be technically difficult to achieve the above goals.

The first challenge arises in the state-of-the-art nanoscale fabrication technique is its inevitable difficulty to achieve deeply sub-wavelength dimension becoming serious. The second chal-lenge lies in material dispersion which is sometimes vital. As we know that metals such as gold, silver, aluminium and copper are highly conductive materials at RF and microwaves, commonly used in conventional circuits. However, at optical frequency, these metals would behave differently, and they exhibit plasmonic resonance instead of the usual conductivity, i.e. the coupling of optical signals with collective oscillation of conductive electrons at these metal surfaces is dominant where the real part of permittivity is negative. In other words, at optical wavelengths, the conduction current is no longer the dominant current circulating through lumped optical elements. Therefore, the traditional circuit theory and the corresponding meth-odology for micro-electronics lose their functionality in optical frequency domain.

In 2007, Engheta et al. have made an important breakthrough and first proposed the concept of 'metatronics' [6] which bridges the gap between low frequency circuitry design and high frequency nanodevice design. In their opinions, it is possible to realize the performance of lumped-circuit-like elements at optical frequency just by properly designing and suitably arranging plasmonic or/and non-plasmonic nanoparticles, as shown in **Figure 1**. The theoret-ical framework of 'metatronics' is very simple and is based on one Maxwell equation $\nabla \times H = J_c + (-i\omega D)$, and this equation has two terms on its right-side: one is the conduction
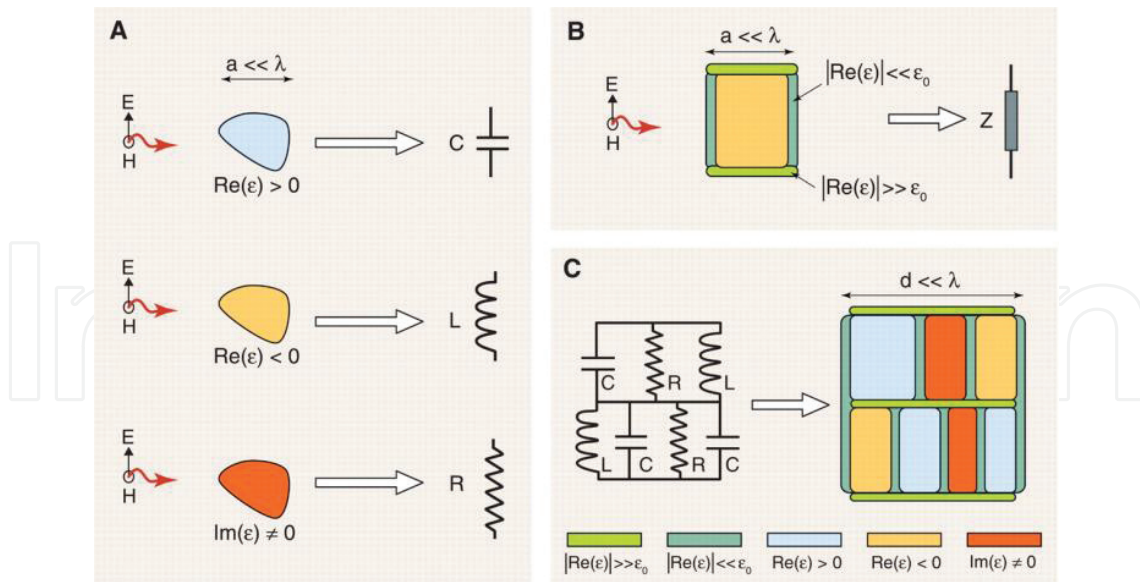
Figure 1. Analogy between sub-wavelength nanoparticles and conventional lumped nanocircuit elements at optical frequency domain. Here, one nanoparticle can take a different role when the sign of its complex permittivity ε is different. If combined in a specific way, different nanoparticles can possess some defined functionalities (adapted from Ref. [6], **Figure 1**).

current $J_c = \sigma E$ and the other is the displacement current $J_d = -i\omega D$. As mentioned above, the material dispersion plays a crucial role at optical wavelength, and the conduction current (originally dominant at low-frequency) is no longer dominant. Instead, the electric displacement current can be taken as the 'flowing optical current'. With the left of displacement current, the next and most important step is to re-build the formulas to calculate the 'lumped impedance' of nanoparticles as for an optical circuit.

2.2. Optical lumped elements

Based on the above 'metatronic' concept, the optical impedance (an intrinsic parameter) of nanoparticles is similar to the electrical counterpart ($Z=V/I$) [8], which is independent of the surrounding environments. As sketched in **Figure 2**, two isolated sub-wavelength nanospheres (radius R) with complex permittivity ε are immersed in homogenous space (with permittivity ε_0 being real) and illuminated uniformly by a vertical electric field E_0. Because of small enough size of nanoparticles (with respect to the central wavelength of illuminating field), the scattered electromagnetic (EM) fields in the vicinity of nanospheres and the total fields inside it can be obtained under suitable approximations by means of the well-known time-harmonic and quasi-static approach [9]. If integrating the flux of displacement current J_d across the sphere induced by the scattered electric field, one can get the 'total' displacement current as,

$$I_{\mathrm{imp}} = I_{\mathrm{sph}} + I_{\mathrm{fringe}} = -i\omega(\varepsilon - \varepsilon_0)\pi R^2|E_0|, \tag{1}$$

$$I_{\mathrm{sph}} = -i\omega\varepsilon\pi R^2(\varepsilon - \varepsilon_0)|E_0|/(\varepsilon - 2\varepsilon_0), \tag{2}$$

$$I_{\mathrm{fringe}} = -i\omega\varepsilon_0 2\pi R^2(\varepsilon - \varepsilon_0)|E_0|/(\varepsilon + 2\varepsilon_0). \tag{3}$$
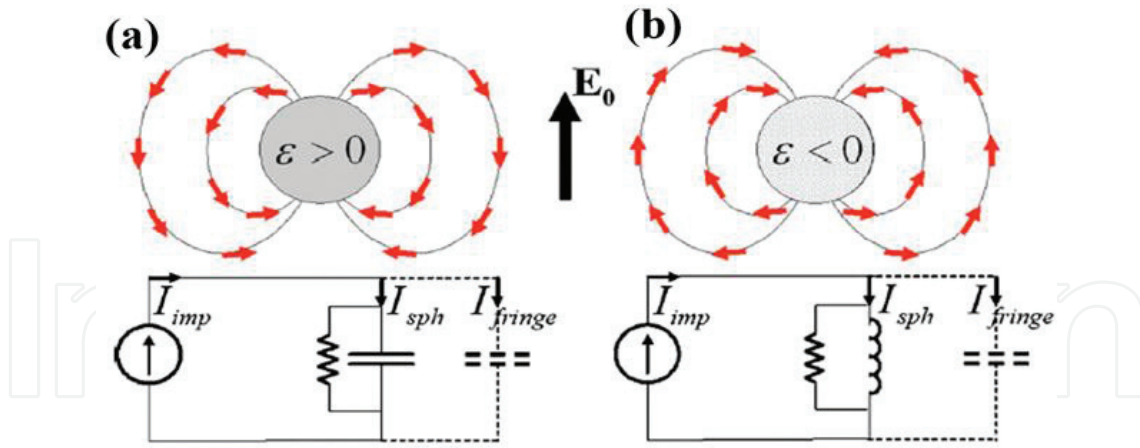
Figure 2. Optical nanocircuit models for (a) dielectric or (b) plasmonic nanoparticles. E_0 denotes the incident electric field, and thinner field lines together with the arrows represent the electric dipolar fringe field from nanospheres. (adapted from Ref. [8], **Figure 1**).

Here, as shown at the bottom of **Figure 2**, I_{imp} is the 'impressed' displacement current, I_{sph} is displacement current circulating in nanospheres and I_{fringe} is displacement current for the fringe (dipolar) field. Such currents are all related to the polarization charges at the surface of nanospheres induced by light source and all can be intuitively interpreted as branch currents at nodes in a parallel circuit.

The 'average' potential difference between the upper and lower hemi-spherical surfaces of the sphere is given by

$$\langle V \rangle_{sph} = \langle V \rangle_{fringe} = R(\varepsilon - \varepsilon_0)|E_0|/(\varepsilon - 2\varepsilon_0) \tag{4}$$

Thus, after having obtained the ratio between the potential difference (Eq. 4) and the effective current evaluated from Eq. (2) or (3), one can, respectively, get the equivalent impedance for the 'nanosphere' or the 'fringe' branch of the circuit as

$$Z_{sph} = (-i\omega\varepsilon\pi R)^{-1}, \quad Z_{fringe} = (-i\omega 2\pi R\varepsilon_0)^{-1}. \tag{5}$$

From Eq. (5), one can clearly see that the two parallel elements in the circuits (**Figure 2**) may behave differently, which is determined by the permittivity sign of the nanospheres as shown in **Figure 1**. For example, a non-metallic (or dielectric) sphere can be thought as a capacitor (because of $(\mathrm{Re}(\varepsilon) > 0)$, parallel with a resistor $(Im(\varepsilon) \neq 0)$, indicating a loss) (left-bottom, **Figure 2**). In contrast, the impedance of the outside fringe is always capacitive, since its permittivity is positive. Therefore, here the equivalent circuit elements are expressed in terms of nanosphere parameters as,

$$C_{sph} = \pi R \mathrm{Re}[\varepsilon], \quad G_{sph} = \pi\omega R \mathrm{Im}[\varepsilon], \quad C_{fringe} = 2\pi R\varepsilon_0. \tag{6}$$

Instead, if such a sphere is made of plasmonic materials (e.g. Ag, Au), it behaves as an inductive element, since $(\mathrm{Re}(\varepsilon) < 0)$, and similarly the equivalent inductor for such a sphere becomes,

$$L_{sph} = (-\omega^2 \pi R Re[\varepsilon])^{-1}. \tag{7}$$

Naturally, one can implement a more complicated circuit by a series and parallel operations among different kinds of such lumped particles. If two nanoparticles share a common interface and electric field is tangential to the common interface, a parallel operation between them would be made effective (left-column, **Figure 3**).

In contrast, if the electric displacement vector locally is normal to that of common interface, the displacement current J_d passing across one element through the common interface must flow inside the second element under the confinement of the continuity condition, and a series cascade of these two nanoelements is realized (right-column, **Figure 3**). This represents an important difference with respect to those in the conventional circuit theory, and in the latter, the lumped elements are completely isolated from the external world, and their interaction with the circuit is determined by the facts that how they pass through their terminals and how they are connected with the rest of the circuit. In contrast, in the former, i.e. the configuration presented here, since the fringing and external fields (**Figure 2**) play dominant roles in the interaction of nanoelements with their neighbouring particles and surrounding environment,
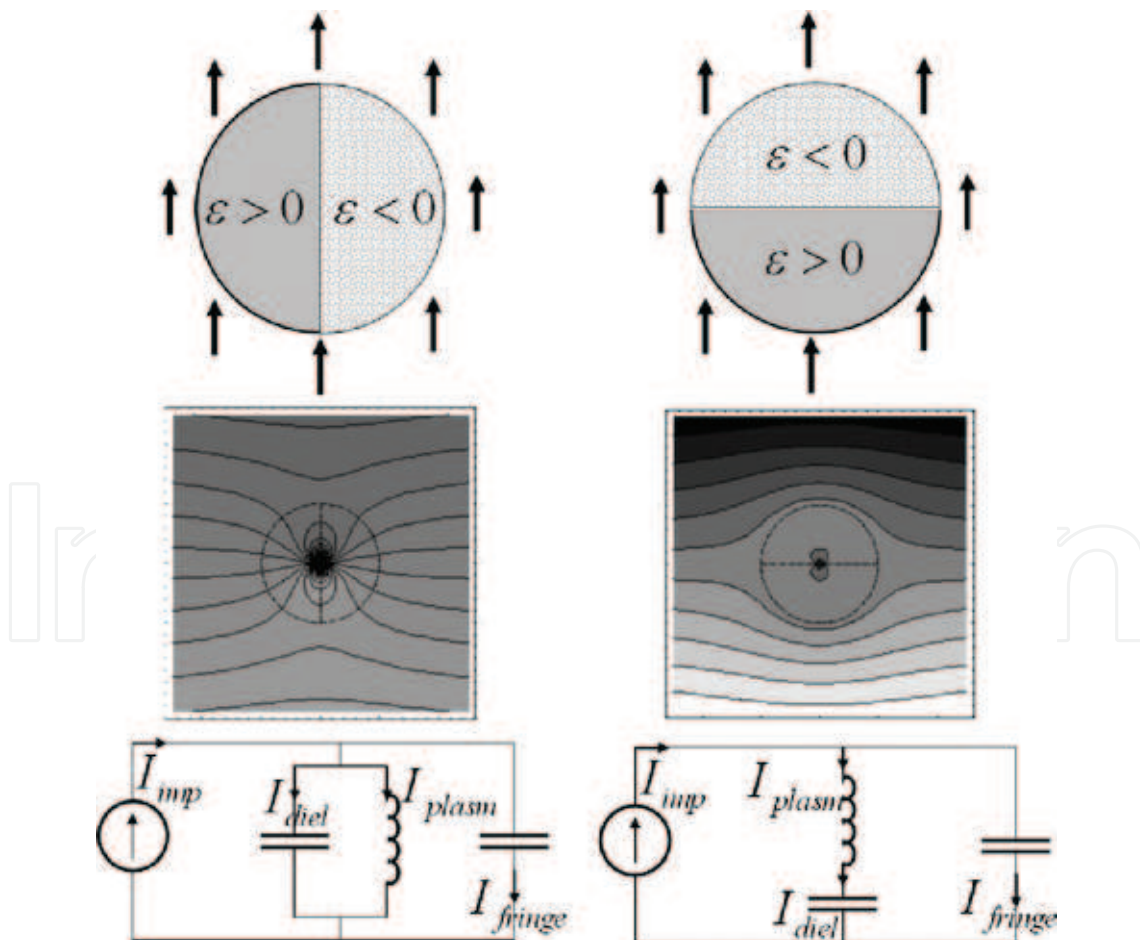
Figure 3. Two conjoined two-dimensional half-spheres with different signs of permittivity, illuminated by a uniform electric field. Parallel (left) and series (right) configurations are, respectively, shown (adapted from Ref. [8], **Figure 2**).

the originally same connection now may consists of both series and parallel interconnections which sensitively depend on the orientation of the external applied field. This point may be taken as an important and additional degree of freedom in optical nanocircuit design.

In the above, just nanosphere is taken as an example particle. In fact, except for this, the basic 'alphabets' of metatronics can also be gratings, cylinder pillars, rectangle bricks and other antennas, and they have been widely applied to various wavelength regimes,for example in a series of theoretical analyses and numerical simulations [4, 7, 10–12].

2.3. Metatronics-based applications

The recent experimental progresses [7, 13] have verified the validity and potentiality of the above optical nanocircuit paradigm introduced in Section 2.2, and also demonstrated the possibility of re-configuring the circuit responses just by changing the orientation and polarization of illuminating field to induce a specific feature not available in conventional electric circuits. No doubt that this metatronics concept provides us an effective and practical tool to design optical nanodevices, such as designing and tuning of optical nanoantennas [14, 15] and meta-surfaces [16].

One representative example is shown in **Figure 4** where a polarization-selective optical filter making use of a simple sub-wavelength grating is designed. Different incident illuminations and different effective optical connections between the nanoelements of this 'stereo-nanocircuit' are chosen to conveniently control the light transmittance, i.e. to make the circuit functions either band-stop or band-pass. This scheme may be exploited for parallel processing of multiple flows of information through a single nanostructure.

In detail, when electric field E is perpendicular to the nanorods (**Figure 4a**), the optical displacement current J_d 'flows' transversely across the nanorods and air gaps (in other words,
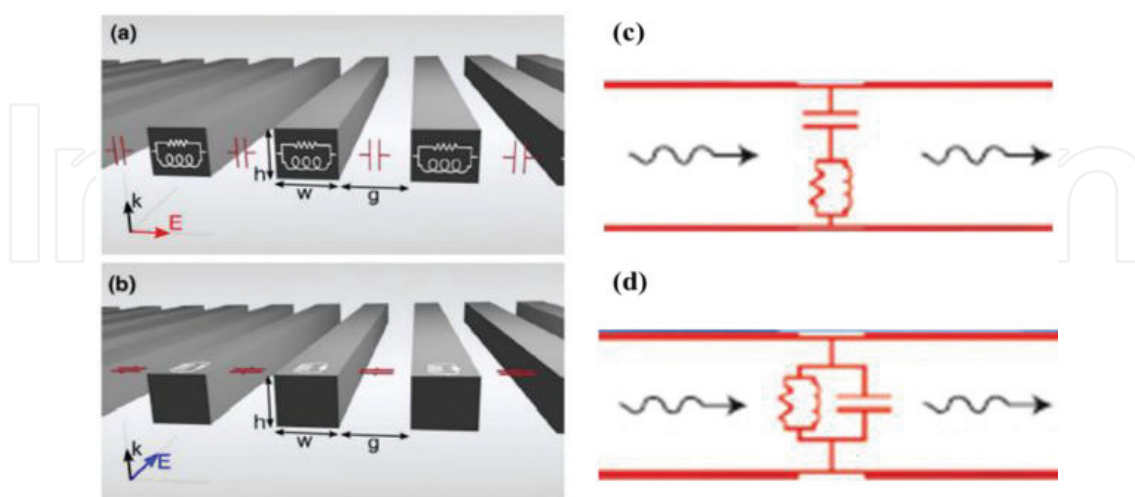
Figure 4. Sub-wavelength grating with parallel plasmonic nanorods working as a two-dimensional optical nanocircuit with a stereo-functionality. (a) The E field is perpendicular to the nanorods and nanoinductors (including nanoresistors) and nanocapacitors form a series configuration (c). In contrast, if the E field is parallel to nanorods (b), a parallel configuration (d) of lumped circuit elements is formed instead (adapted from [10], **Figure 1**).

the displacement current is in the plane of the arrays but perpendicular to the nanorods). Therefore, the final equivalent series impedance is written as,

$$Z_{\perp(\text{equivalent})} = Z_{\perp(\text{nanorod})} + Z_{\perp(\text{airgap})},$$
$$Z_{\perp(\text{nanorod})} = iw/\omega h\varepsilon, \quad Z_{\perp(\text{airgap})} = ig/\omega h\varepsilon_{\text{air}}. \tag{8}$$

In contrast, when E is parallel to the nanorods (**Figure 4b**), the optical displacement current J_d 'flows' along both the nanorods and air gaps. Therefore, each nanorod and its neighbouring air gap collectively have equivalent parallel impedance,

$$Z_{\|(\text{equivalent})} = Z_{\|(\text{nanorod})}Z_{\|(\text{airgap})}/(Z_{\|(\text{nanorod})} + Z_{\|(\text{airgap})}),$$
$$Z_{\|(\text{nanorod})} = i/\omega wh\varepsilon, \quad Z_{\|(\text{airgap})} = i/\omega gh\varepsilon_{\text{air}} \tag{9}$$

These equivalent impedances (series or parallel, in Eqs. (8) and (9)) finally determine the transmittance of the incident optical signal, and the latter is naturally derived as,

$$T_{\perp} = |Z_{\perp(\text{equivalent})}/(Z_{\perp(\text{equivalent})} + [\eta_0(w+g)/2])|^2,$$
$$T_{\|} = |Z_{\|(\text{equivalent})}/(Z_{\|(\text{equivalent})} + [\eta_0/(2(w+g))])|^2. \tag{10}$$

To test this optical circuit approach, one can compare the results in **Figure 5** calculated from Eq. (10) with those experimentally measured (10) or exactly numerical results with the help of
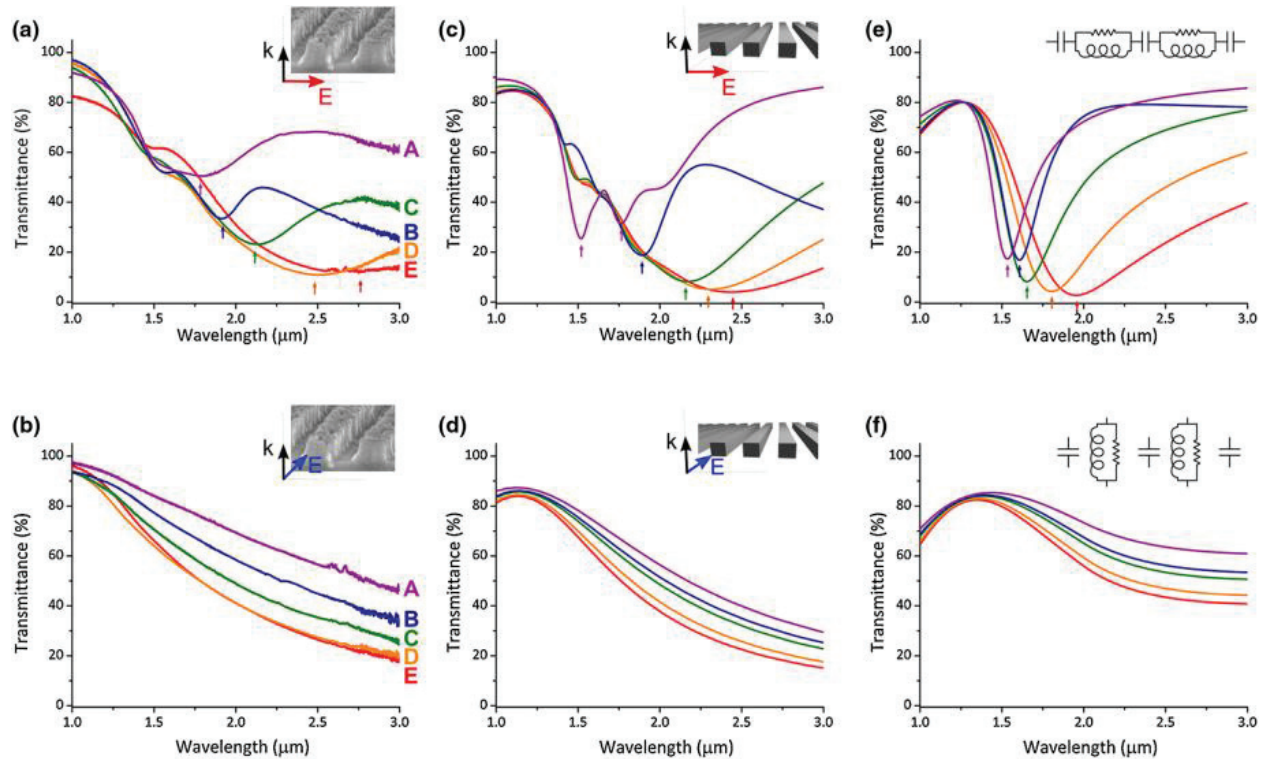

Figure 5. Transmittance spectra for five different samples from A to E. Experimentally measured data for (a) perpendicular or (b) parallel polarization of the incident wave impinging on the nanorod arrays. (c and d) Full-wave simulation results and (e and f) calculation results from nanocircuit theory for polarization perpendicular (upper) or parallel (lower) to nanorods (adapted from Ref. [10], **Figure 2**).

a commercial software. As one expects, the grating with a 'series' configuration behaves as a band-stop filter, however the same grating with a 'parallel' configuration as a band-pass filter instead.

Another representative example is related to the radio-frequency (RF) antennas which have been widely investigated and applied in wireless telecommunication system in the last century. The functionality of RF antenna is information revolution. It is usually used with a radio transmitter or radio receiver. In transmission, a radio transmitter supplies an electric current oscillating at radio frequency (i.e. a high frequency alternating current (AC)) to the antenna's terminals, and the antenna radiates the energy from the current as electromagnetic waves (radio waves). In analogy with their RF counterparts, optical antennas made of plasmonic nanoparticles are able to efficiently coupled localized sources or guided waves at the nanoscale level to far-field radiation, and in turn, to convert the impinging radiation from the far-field into sub-wavelength localized or guided fields [17]. As the counterpart of RF antenna, an optical nanoantenna exhibits novice and interesting characteristics because of their plasmonic nature.

In detail, as depicted in **Figure 6a**, a conventional linear RF antenna is loaded at its feeding gap with lumped circuit elements and changing the antenna input impedance allowance to operate at a given frequency or to achieve a good match for a specific feeding network. Analogously, an optical nanocircuit opens the same possibility for an optical nanoantenna (**Figure 6b**), and the complex optical input impedance can be interpreted as the parallel combination of the dipole intrinsic impedance Z_{dip} and the gap impedance Z_{gap} [11, 15]. The former impedance is assumed to be a fixed property of the nanoantenna geometry and surrounding environment, and the latter can be engineered to a large extent by loading the gap with different materials.
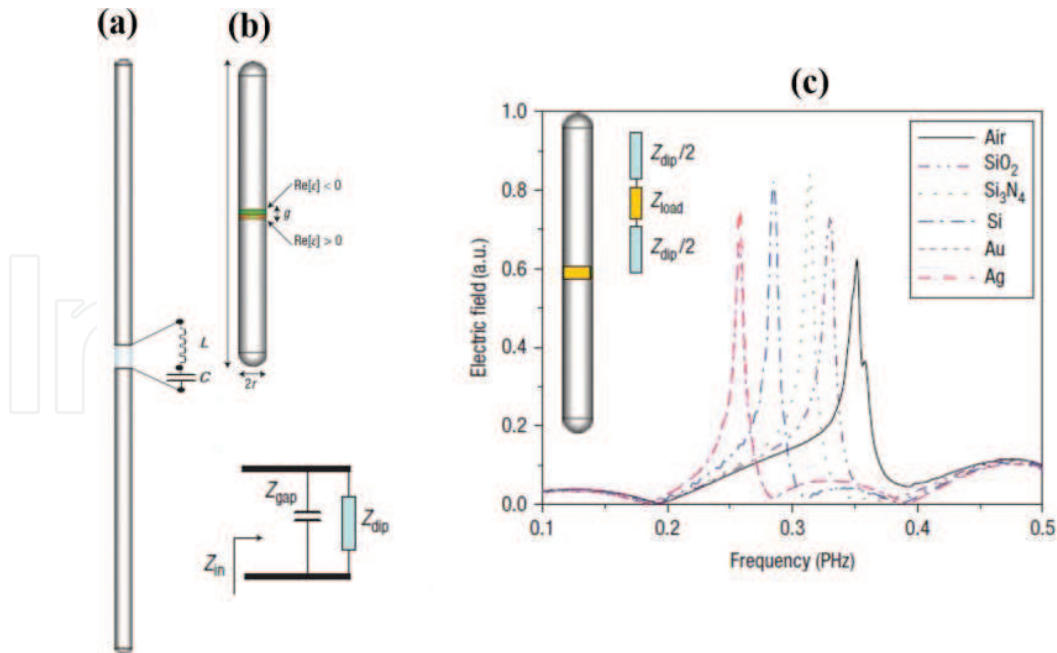

Figure 6. Optical nanoantennas. RF dipole antenna (a) loaded with lumped circuit elements at its feeding gap, and analogously, a plasmonic dipole nanoantenna (b) loaded with optical nanocircuits (adapted from Ref. [15], **Figure 1**). The low inset shows the circuit model of antenna input impedance. (c) Tuning of nanoantenna resonance by 'gap loading' with different realistic materials (adapted from Ref. [15], **Figure 3**).

Such as for a cylindrical gap with height of t, radius of a and excited by an incident electric field parallel to its axis, the gap impedance is given by,

$$Z_{gap} = \frac{it}{\omega \varepsilon \varepsilon_0 \pi a^2}. \tag{11}$$

Thus, by filling the gap with different materials (or their proper series or parallel combination), the impedance of the gap can be tailored to a large degree. As a result, one can tune the frequency response (**Figure 6c**) or radiation pattern easily.
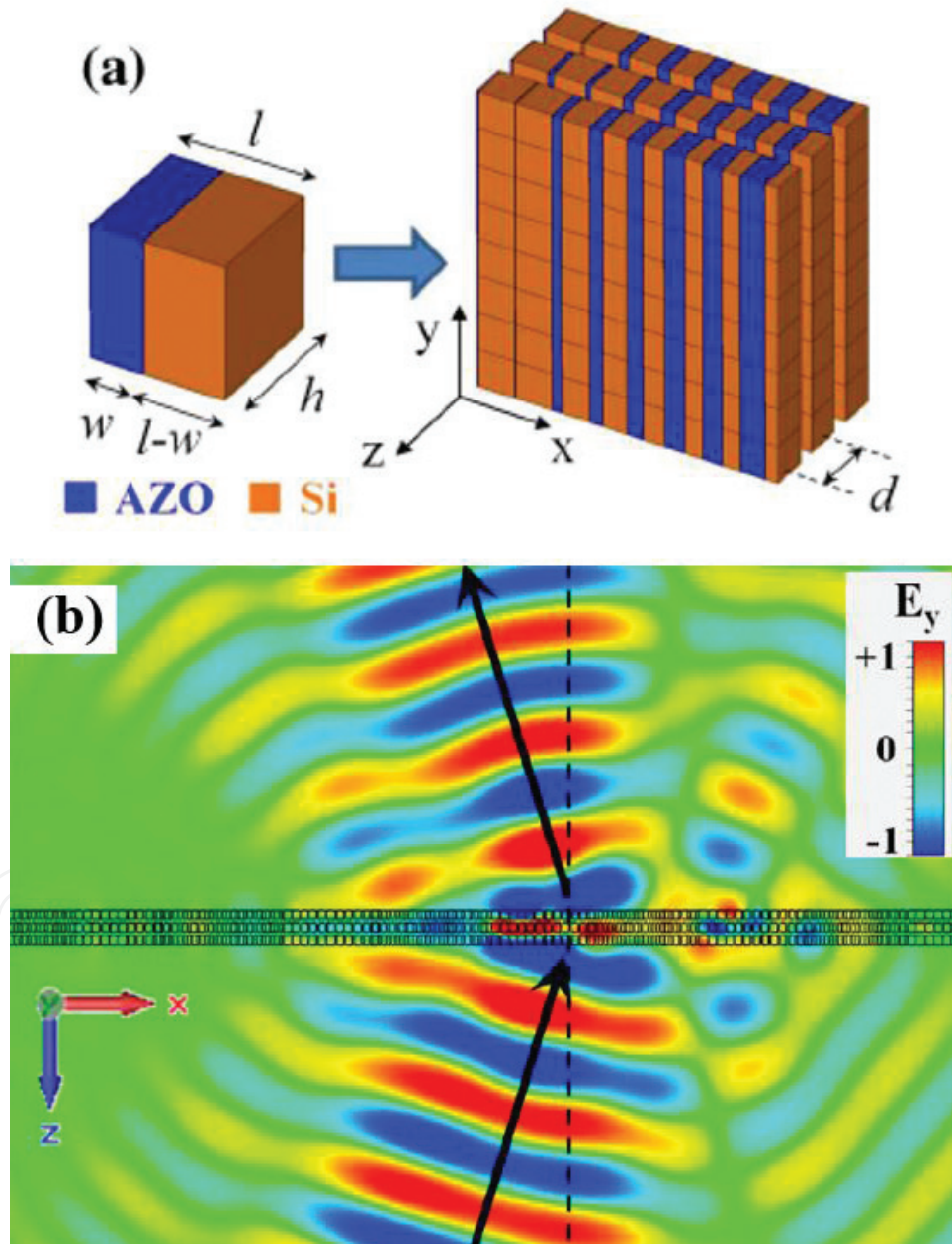
Figure 7. Meta-transmit-array used for full control of nanoscale optical transmission. (a) Basic nanocircuit building block (left) and resulting meta-screen (right) with transverse inhomogeneous profiles of surface impedance. (b) Full-wave simulation of meta-transmit-array for light deflection with high efficiency and minimized reflection (adapted from Ref. [16]).

In addition, except for the above sub-wavelength grating and non-antenna, meta-surface represents another important type [18], the planar counterparts of meta-materials that provide the unprecedented control of the amplitude, phase or polarization of light waves at the sub-wavelength (nano) scale. For example, these two-dimensional surfaces can alter the wave-front of incident light for a widespread application in beam shaping [19–24], polarizers [25, 26] and flat lenses [27–29]. As proposed in [16], the fundamental building blocks are paired plasmonic or dielectric nanorods collectively working as an inductor–capacitor nanocircuit (**Figure 7a**, left), whose impedance depends directly on the filling ratio of plasmonic and dielectric materials. By suitably alternating these nanocircuit blocks on the transverse direction, one can synthesize a meta-surface with the required inhomogeneous impedance profile. The configuration composed of a stack of three meta-surfaces (**Figure 7a**, right), can fully control the nanoscale optical transmission, while simultaneously minimizing the reflection (impedance-matching to free-space), allowing, for example light deflection with an almost ideal efficiency as shown in **Figure 7b**.

3. Equivalent nanocircuit theory for multi-layer meta-material design

In this Section, the 'design stack' is moved upward, from the 'physical layer' of optical lumped elements (pure nanoparticles, nanogratings, nanoantennas, etc.) to more complex functional devices, including: (1) infrared third-order Butterworth filters; (2) metal-insulator-metal (MIM) ultra-broadband absorbers; (3) simplified broadband super-flat perfect infrared absorbers only composed of single transparent conductive oxides (TCOs). Among these design procedures for multi-layer nanostructures in our research group, the suitability of the equivalent nanocircuit theory is confirmed once more which in turn enriches and expands the application of equivalent nanocircuit theory.

## 3.1. Infrared broadband third-order Butterworth filters

Frequency selective surfaces (FSSs) have been the subject of investigations by many researchers for decades. An FSS is a periodic structure usually composed of an assembly of identical elements arranged in one- or two-dimensional lattice. These structures are used in a variety of important applications ranging from microwave systems and antennas to radar and satellite communications. The simplest FSS device is a filter. By means of circuit elements (e.g. resistors (R), inductors (L) and capacitors (C)) FSSs can be effectively and flexibly designed to functionalize a low-pass, high-pass, band-pass or band-stop responses in the microwave or RF domain [30, 31]. The great interests in FSS's application in higher frequency range to achieve high-density and high-speed optical analogues [5, 10] have been pushed and the goals have been synthesized as realistic nanostructures at optical frequency, thanks to the optical nanocircuit theory which proves once more to be an essential design tool to construct optical FSSs or filters.

Different from those basic 'alphabets' mentioned in the previous section (nanogratings, nanoantennas, etc.), here, nanobricks are chosen as the building blocks. One reason is that they

are widely used as the atoms of meta-material and plasmonic structure, and the second is that the brick's planar profile makes us easily calculate the equivalent impedance.

As a demonstration, one layer of periodic nanosquare array based on indium-tin-oxide (ITO) used for an infrared FSS filer is presented (**Figure 8**). The reason why ITO material is chosen for making up of FSS filter cells is just that, it possesses low electrical resistance and high transmittance in the visible range and widely used as an electrode for displays [33]. Especially, in the infrared spectral range, ITO material can demonstrate a metallic performance and this makes it to become a counterpart of noble metal. In addition, in the practical calculations, the permittivity ITO is usually modelled by the Drude dispersion relation.

When such a nanosquare array is illuminated vertically (along z-direction) by an optical signal from the bottom side with electric field E polarized parallel to the x-direction, the optical displacement current J_d 'flows' along both the unit cells and air gaps [7, 32], the nanosquare array first acts as a 'parallel' combination of lumped elements R, L and C_1, and then in series with a capacitance C_2, as shown in **Figure 8b**. Following the general capacitor impedance formula $Z_c = i/(\omega C)$ with the capacitance $C = \varepsilon a/b$, and a, b being the element's two-dimensions, the effective lumped impedance of the unit nanosquare cells can be written as,
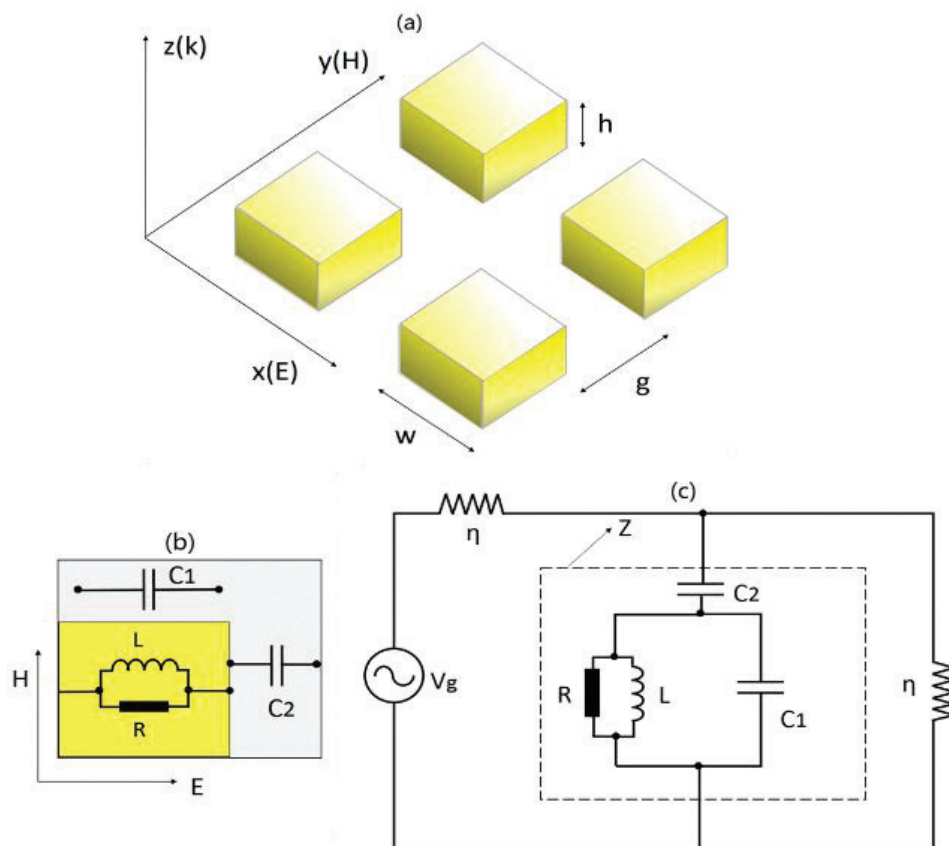
Figure 8. Schematic diagrams of (a) periodic nanosquare array (as for its unit cell, the width and height, as well as the gap distance between two adjacent unit cells are denoted as w, h and g), (b) equivalent lumped circuit elements and (c) whole equivalent circuit used for designing single-layer FSS filter (adapted from Ref. [32], **Figure 1**).

$$Z_{\text{ITO}} = Z_R \| Z_L = iw/\omega hw\varepsilon_{\text{ITO}},$$
$$Z_{C_1} = iw/\omega hg\varepsilon_{\text{air}}, \quad Z_{C_2} = ig/\omega h(w+g)\varepsilon_{\text{air}} \tag{12}$$

Thus, the input impedance of a single layer is given by,

$$Z = Z_{\text{ITO}} \| Z_{C_1} + Z_{C_2}. \tag{13}$$

Subsequently, the equivalent circuit model of this whole FSS system (**Figure 8c**), where $\eta = \sqrt{\mu/\varepsilon}$ is the intrinsic impedance of surrounding medium. Within the equivalent circuit impedance theory [34], the reflectance and transmittance of the incident optical signal are naturally obtained as,

$$S_{11} = (Z\|\eta - \eta)/(Z\|\eta + \eta), \quad S_{21} = S_{11} + 1,$$
$$R = |S_{11}|^2, \quad T = |S_{21}|^2 = |2Z/(2Z+\eta)|^2. \tag{14}$$

Obviously, in order to achieve different optical responses, the impedances of nanocircuit elements can be changed, by tuning the structural size (w, h or g), the constituent material property (ε_{ITO}), or the illumination light wavelength ($\lambda = 2\pi c/\omega$) and then the property of such a band-stop filter could be flexibly controlled. As a demonstration, samples from A to D with different widths of 100, 200, and 300 nm, but with fixed gap of 100 nm and height of 150 nm for simplicity are chosen.

The transmittances of the FSS filters composed of samples from A to D, shown in **Figure 9a**, are obtained through Eq. (14). In addition, one can employ a full-wave FDTD simulation to check the validity of such an equivalent nanocircuit theoretical model, and the corresponding transmittance spectra are shown in **Figure 9b** for comparison. The comparison result indicates that they are consistent well with each other.

As investigated in **Figure 9c**, the band-stop behaviour of the FSS filters is dependent on their geometric size. With the increment of w/g, the band-stop centre has a red-shift which can be well interpreted by the optical circuit theory [15]: the larger the width of the nanosquare unit cell, the bigger the inductor L induced between the two adjacent air gaps, hence leading to a higher resonant wavelength. In contrast, with the increment of w/g, the band-stop depth decreases and this behaviour is a result of the fact that the larger the width of nanosquare unit cell the stronger the guidance of light. From the electric field distribution for one representative sample at the resonance frequency, one can see that the unit cell structure works as an antenna and the incident light is localized at the regions between two adjacent metal unit cells, resulting in significant resonant enhancement of localized field and a guidance of most light through the air gap [35, 36].

As for a more practical and wide application, a flatter and broader band-stop filtering response curve with a fast roll-off would be much advantageous [37]. To gain this aim, as the general FSS-based filter design scheme does [38, 39], a third-order Butterworth band-stop filter is realized by cascading triple-layer of nanosquare unit cells with a specific separation distance D between the consecutive layers (**Figure 10a**). The corresponding equivalent circuit is modelled in **Figure 10b**. Then, the whole structure is separated into four regions along the
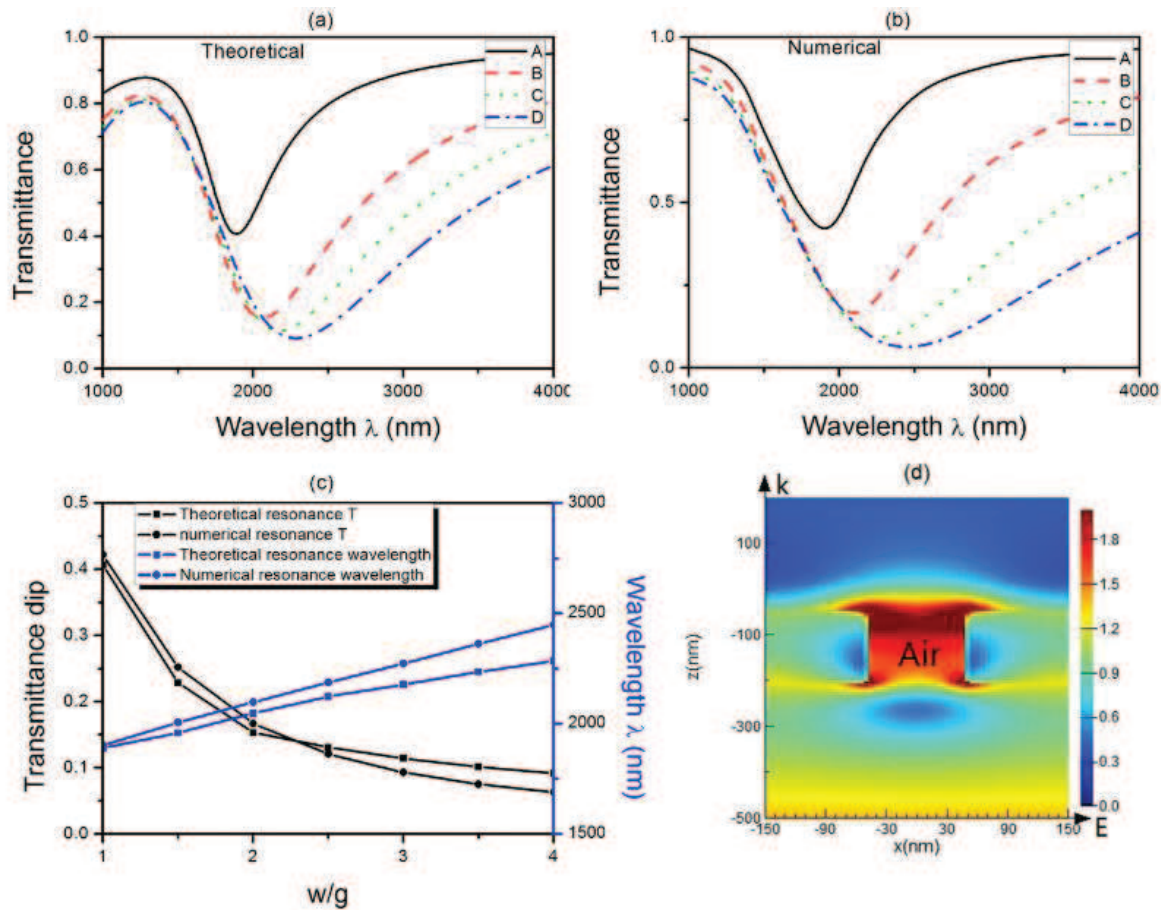
Figure 9. (a) Theoretical and (b) numerical transmittance spectra based on equivalent circuit theory and FDTD simulation for samples from A to D, respectively. (c) The resonance wavelength and transmittance dip as a function of w/g. (d) The representative electric field distribution for sample B at resonance wavelength (adapted from Ref. [32], **Figure 2**).

propagation direction (**Figure 10c**). Finally, along the similar procedure, the transmittance T after the third layer can be obtained step by step.

(1) As for the first layer, the theoretical S-parameters are

$$S_{11} = \frac{Z_1\|\eta - \eta}{Z_1\|\eta + \eta} \quad , \quad S_{21} = S_{11} + 1, \quad S_{22} = S_{11}, \quad S_{12} = S_{21}. \tag{15}$$

Here, the impedance of the surrounding medium above or between the neighbouring layers is η and that of each layer is Z_i (i = 1, 2, 3). As for the second or third layer, the S-parameters (S_{33}, S_{43}, …) can be get by just replacing Z_1 in Eq. (15) with Z_2 or Z_3.

(2) The reflected power P_{iR} and transmitted power P_{iF} from each layer are evaluated as follows,

$$\begin{aligned}
P_{1R} &= |S_{11}|^2 P_{1F} + |S_{12}|^2 P_{2R}, & P_{2F} &= |S_{21}|^2 P_{1F} + |S_{22}|^2 P_{2R}, \\
P_{2R} &= |S_{33}|^2 P_{2F} + |S_{34}|^2 P_{3R}, & P_{3F} &= |S_{43}|^2 P_{2F} + |S_{44}|^2 P_{3R}, \\
P_{3R} &= |S_{55}|^2 P_{3F}, & P_{4F} &= |S_{65}|^2 P_{3F}.
\end{aligned} \tag{16}$$

For simplicity, the absorption loss caused by the surrounding medium is assumed negligible.
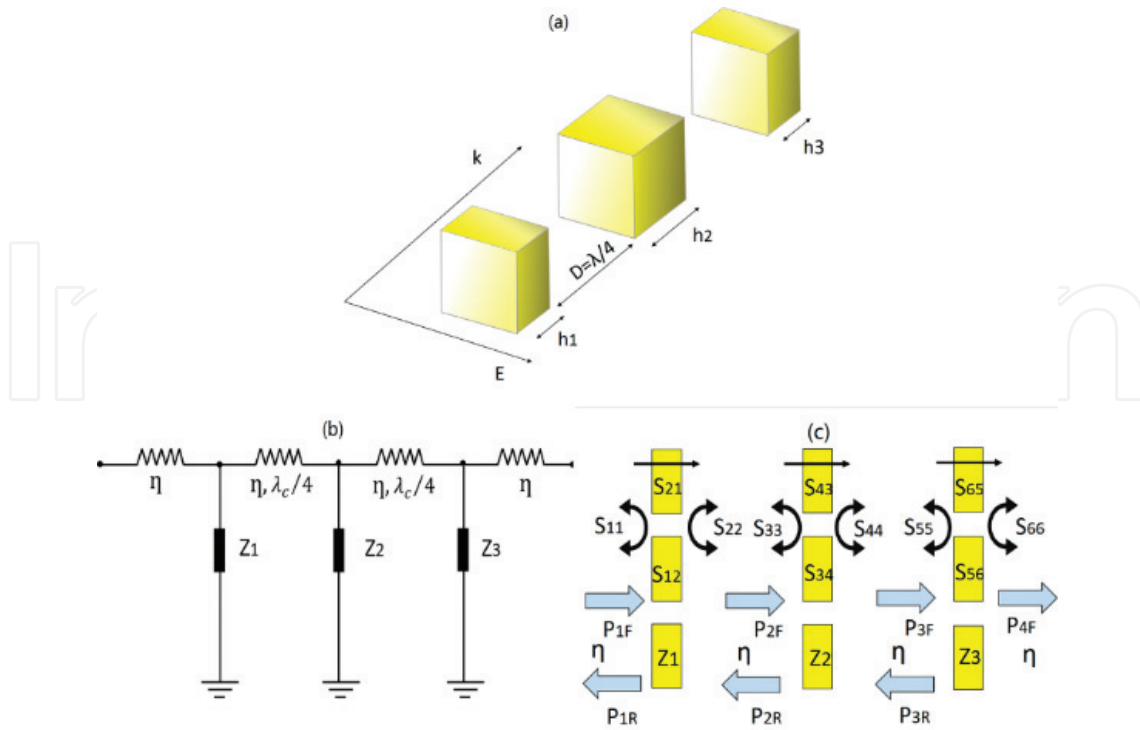
Figure 10. Schematic diagrams of (a) triple-layer FSS filter, (b) equivalent circuit and (c) S-parameters (adapted from Ref. [32], **Figure 3**).

(3) The total transmittance after the third layer is then written as

$$T = P_{4F}/P_{1F} = \frac{|S_{21}|^2|S_{43}|^2|S_{65}|^2}{1 - |S_{11}|^2|S_{33}|^2 - |S_{33}|^2|S_{55}|^2 + |S_{11}|^2|S_{33}|^4|S_{55}|^2 - |S_{11}|^2|S_{43}|^2|S_{55}|^2}. \quad (17)$$

As for any specific third-order Butterworth filter with desired central band-stop frequency and band-stop width, one can easily get the suitable choice of geometrical parameters for design. For example, if the band-stop edge frequencies are ω_1 and ω_2, the central frequency can be defined as $\omega_0 = \sqrt{\omega_1\omega_2}$ and band-stop width as $\omega_b = (\omega_2 - \omega_1)/\omega_0$. The reactance slope parameters of this circuit model in terms of low-pass prototype parameters G_0, G_1, ..., G_{n+1} and cut-off frequency ω_c are given as [34]

$$\frac{Z_i}{Z_0} = \frac{G_0}{\omega_c G_i \omega_b} \text{ if } n = \text{even;} \quad \frac{Z_i}{Z_0} = \frac{1}{\omega_c G_0 G_i \omega_b}, \text{ if } n = \text{odd.} \quad (18)$$

Here, G_i is the normalized prototype element values and n is the order of the Butterworth filter, that is the number of resonators. As for a third-order (n = odd) band-stop filter (G_1 = 1, G_2 = 2, G_3 = 1) with the height of nanosquare cells at each layer $h_1 = 1/2h_2 = h_3$ fixed, the impedance of each layer (**Figure 10b**) can be obtained as $Z_1 = 2Z_2 = Z_3 = \eta/(\omega_c\omega_b)$.

As for this triple-layer third-order filter, if adopting parameters listed in **Table 1**, the theoretical and numerical transmittance spectra can be directly obtained (**Figure 11a**) based on Eq. (17) from an equivalent circuit theory and FDTD simulation, respectively. The comparison between

i	G_i	Z_i	w/g (nm)	h_i (nm)
1	1	Z	120/60	150
2	2	Z/2	120/60	300
3	1	Z	120/60	150

Table 1. Element values for low-pass prototype circuit and geometrical parameters of third-order band-stop FSS filter.
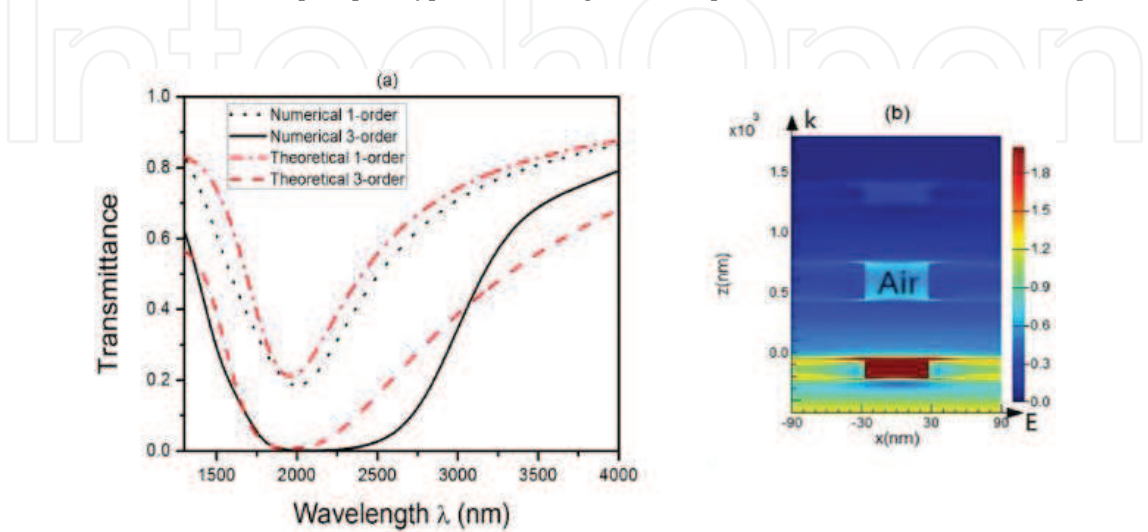
Figure 11. (a) Theoretical and numerical transmittance spectra for single-layer (first-order) or triple-layer (third-order) filter. (b) One representative electrical field distribution for a third-order filter at a wavelength of 2000 nm (adapted from Ref. [32], **Figure 4**).

single-layer and triple layer filters indicates that, for a triple-layer filter, its band-stop width and depth both become larger, and moreover, its band-stop bottom is much flatter. In addition, the transmittance is nearly zero, indicated by the electric field distribution in **Figure 11b**.

It is necessary to point out that the corresponding FDTD calculation results show a good agreement with for single-layer case, but more obvious deviation from the equivalent circuit theoretical calculation. The reason for deviation arises from the simple assumption that the triple-layer of nanosquare array is independent of each other. If the layer-layer coupling is considered the deviation maybe reduced. However, anyway, the proposed synthesis procedure is confirmed helpful to design a Butterworth band-stop filter.

### 3.2. Infrared broadband multi-layer MIM absorbers

Meta-material absorbers are used broadly in thermal detectors [40], imaging [41], security detection [42] and stealth devices [43]. In 2008, Landy et al. first proposed a thin perfect meta-material absorber simultaneously exciting electric and magnetic resonances (MRs) to realize the impedance match with the surrounding medium and thus eliminating any reflection and perfectly absorbing the incident waves at microwave bands [44]. Since then, applications to various wavelength regimes have been demonstrated widely by numerical simulations and experiments [45, 46]. However, the application of these perfect absorbers is limited for their narrowband and simple resonant behaviours.

The most widely used scheme [47–49] instead is to slow down the incident wave or totally absorb them by a gradually changed pyramid-shaped metal-insulator-metal (MIM) topology (**Figure 12a**). In fact, an absorber can also be thought as a filter, by operating the frequency response of the absorptance with $A = 1 − T − R$. Furthermore, each layer of the multi-layer MIM absorber projecting to the bottom plane is a nanosquare structure (**Figure 12b**), same as basic building blocks for third-order Butterworth filter (Section 3.1). Thus, naturally, the equivalent nanocircuit procedure can be directly transplanted to the design of MIM multi-layer absorber.

The first step is to evaluate the impedance Z (**Figure 12c**) of each layer, following the same procedure in Section 3.1 which can be obtained as,

$$Z_{ITO} = Z_R \| Z_L = iw/\omega hw\varepsilon_{ITO}, \quad Z_{C_1} = iw/\omega hg\varepsilon_{air},$$
$$Z_{C_2} = ig/\omega h(w + g)\varepsilon_{air}, \quad Z = Z_{ITO} \| Z_{C_1} + Z_{C_2}. \tag{19}$$

The second step is to cascade the impedance of each layer into a whole circuit, for example that of a triple-layer structure. Each layer is separated by one quarter of central wavelength of the incident light (**Figure 12a**). The corresponding equivalent circuit can be modelled as in **Figure 12b**, where $\eta = \sqrt{\mu/\varepsilon}$ is the intrinsic impedance of SiO_2 dielectric layers, and Z_i (i = 1, 2, 3) is the impedance of each NS layer. Within transmission line theory [34], $Z(3)$ is the effective impedance
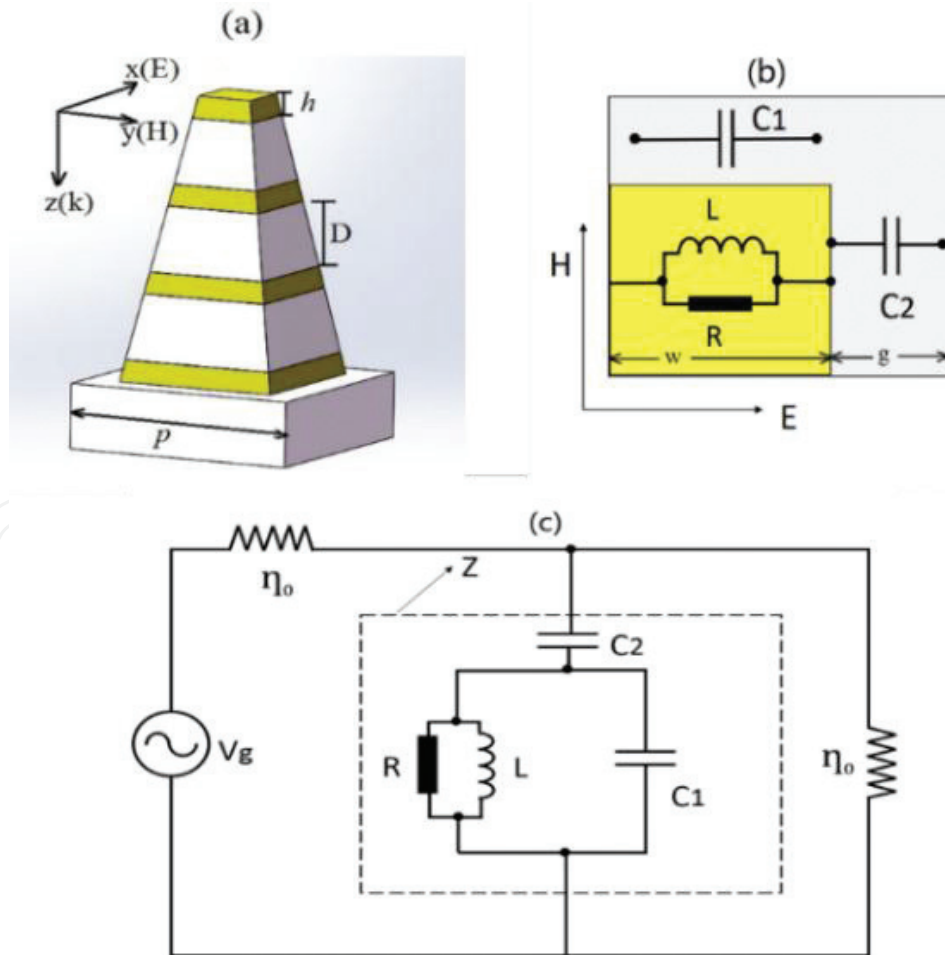
Figure 12. Schematic diagrams of (a) MIM absorber, (b) equivalent lumped circuit elements and (c) whole equivalent circuit. Here, only single nanosquare patch layer is considered (adapted from Ref. [50], **Figure 1**).

at the top interface of the third NS layer, given by $Z(3) = Z_3 \| \eta$. Similarly, for the interface at the second or first layer, the effective impedances can be written as,

$$Z(2) = Z_2 \| (\eta^2 / Z(3)) , \qquad Z(1) = Z_1 \| (\eta^2 / Z(2)) \tag{20}$$

Then, the reflectance of this pyramid triple layer structure is given by,

$$R = \left| \frac{Z(1) - \eta_0}{Z(1) + \eta_0} \right|^2 . \tag{21}$$

Beyond the reflectance, one needs to calculate the transmittance through the bottom substrate. As shown in **Figure 13a**, based on the three different NS layers, the whole structure is separated into four independent regions from left to right. Then, the S-parameters (S_{11}, S_{21}, …) for each layer are obtained as follows,
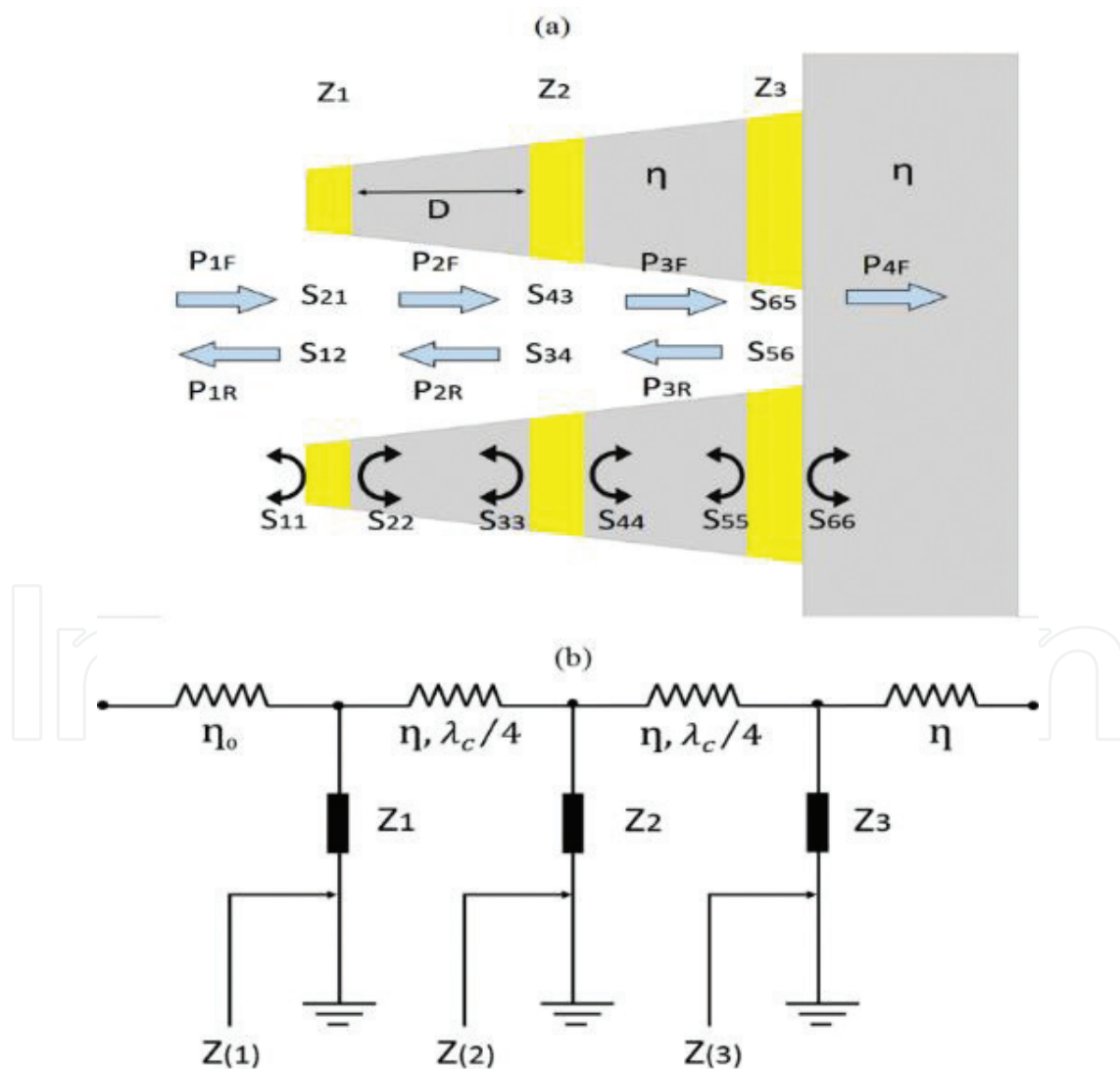
Figure 13. Schematic diagrams of (a) S-parameters used for theoretical calculation and (b) equivalent nanocircuit model for the truncated pyramid triple-layer absorber (adapted from Ref. [50], **Figure 3**).

$$S_{11} = S_{22} = \frac{Z_1 \| \eta - \eta_0}{Z_1 \| \eta + \eta_0}, \quad S_{21} = S_{12} = S_{11} + 1,$$

$$S_{33} = S_{44} = \frac{Z_2 \| \eta - \eta}{Z_2 \| \eta + \eta}, \quad S_{43} = S_{34} = S_{33} + 1, \quad (22)$$

$$S_{55} = S_{66} = \frac{Z_3 \| \eta - \eta}{Z_3 \| \eta + \eta}, \quad S_{65} = S_{56} = S_{55} + 1.$$

For the convenience of calculation, the dielectric loss for light through SiO_2 material is neglected as long as the gap distance between two adjacent layers is large enough. Under this simplification, the reflected power P_{iR} and transmitted power P_{iF} from each NS layer are evaluated as follows,

$$
\begin{aligned}
P_{1R} &= |S_{11}|^2 P_{1F} + |S_{12}|^2 P_{2R}, & P_{2F} &= |S_{21}|^2 P_{1F} + |S_{22}|^2 P_{2R}, \\
P_{2R} &= |S_{33}|^2 P_{2F} + |S_{34}|^2 P_{3R}, & P_{3F} &= |S_{43}|^2 P_{2F} + |S_{44}|^2 P_{3R}, \\
P_{3R} &= |S_{55}|^2 P_{3F}, & P_{4F} &= |S_{65}|^2 P_{3F}.
\end{aligned}
\quad (23)
$$

Solving Eqs. (22) and (23) simultaneously, the total transmittance T is finally expressed as,

$$T = P_{4F}/P_{1F} = \frac{|S_{21}|^2 |S_{43}|^2 |S_{65}|^2}{1 - |S_{11}|^2 |S_{33}|^2 - |S_{33}|^2 |S_{55}|^2 + |S_{11}|^2 |S_{33}|^4 |S_{55}|^2 - |S_{11}|^2 |S_{43}|^2 |S_{55}|^2}. \quad (24)$$

Naturally, the absorptance A can be evaluated as,

$$A = 1 - R - T. \quad (25)$$

The absorption (A), reflection (R) and transmission (T) spectra calculated by above equations and corresponding FDTD simulations, shown in **Figure 14a**, show a good agreement between
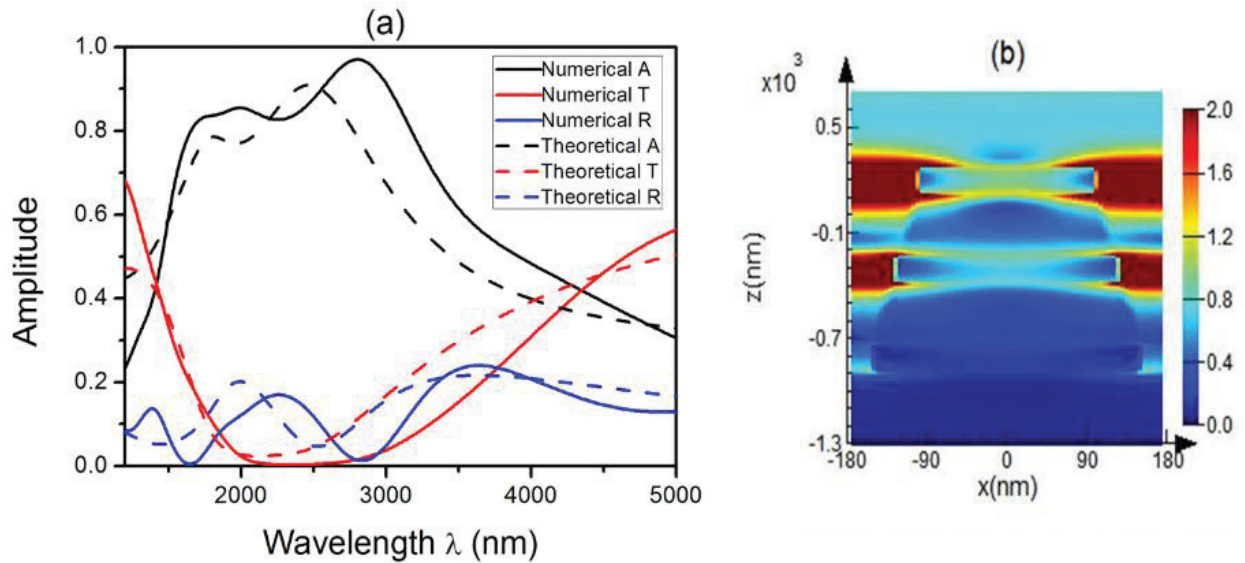
Figure 14. (a) Comparison between theoretical results from equivalent nanocircuit theory and numerical calculations from FDTD simulation. (b) Electric field distribution at a wavelength of 2500 nm. Each nanosquare S patch has a varying width w of 300, 250 and 200 nm from bottom to top (adapted from Ref. [50], **Figure 4**).

the two existing methods which further prove the feasibility of our equivalent circuit theory. The replacement of single-layer absorber by a triple-layer makes the absorptance bandwidth to become obviously wider and also the efficiency is significantly enhanced. The enhanced electric field (**Figure 14b**) concentrates at both the lateral edges of NS and air gaps between two adjacent unit cells that couples efficiently to the incident light and dissipate the energy within the metals via Ohmic loss [51]. After the third layer, nearly no light can be transmitted from the absorber.

3.3. Simplified broadband super-flat perfect absorber

In Section 3.2, a triple-layer MIM absorber design has been successfully demonstrated based on the equivalent nanocircuit theory. The proposed synthesis circuit procedure is confirmed to be feasible enough to provide us a way to predict the responses of such absorbers. It need to be emphasized that, it is in principle possible to get a perfect absorber with a 100% absorption efficiency just by adding more NS layers beyond three layers. However, with the increase of NS layer number, the equation number contained in Eqs. (22) and (23) will be added. Correspondingly, solving the multi-variable linear equations becomes more and more complicated and also time consuming which would be a big problem.

Thus, in this section, an improved equivalent nanocircuit matrix algorithm emerges as the times requires [52] which can predict the complex frequency response of multi-layer (with arbitrary layer numbers) nanostructures easily, without solving the multi-variable linear equations. One can believe that it may provide inspiring advancements in future meta-material designs.

The construction of this equivalent nanocircuit matrix algorithm derives from the design of a simplified broadband super-flat perfect absorber made of single transparent conductive oxides (TCOs) material [52]. In such an absorber design [53], in order to pursue a broadband flat response, until now, no matter how many layers, the multi-layer MIM absorber or planar multiplexed pattern absorber still cannot achieve broadband flat perfect absorption as one expects. Furthermore, there has another challenge for these kinds of broadband absorber design which is related to the fabrication process. It is hard to scale down to higher frequency mainly because of the fabrication difficulty, including lithography and alignment between neighbouring layers or resonators. Within this context, one should explore new paradigms for broadband absorber design.

Fortunately, we note that the transparent conductive oxides (TCOs), such as Al:ZnO (AZO), Ga:ZnO (GZO) and indium-tin-oxide (ITO), can play a fascinating role in the designing of broadband perfect absorber for its unique transmission or conductive property in near-infra-red (NIR) region [33, 53]. As shown in **Figure 15a**, periodic arrays of truncated pyramid structure made of TCOs could work as a broadband absorber in NIR frequency, furthermore such absorbers at broadband wavelengths have continuous flat responses with near-unit light absorption. Comparing with the traditional multi-layer metal-insulator-metal (MIM) absorber, TCOs absorbers using only one single material can greatly reduce the fabrication difficulty, one do not need to consider the perfect alignment to match the relative position of each pattern in different layers.
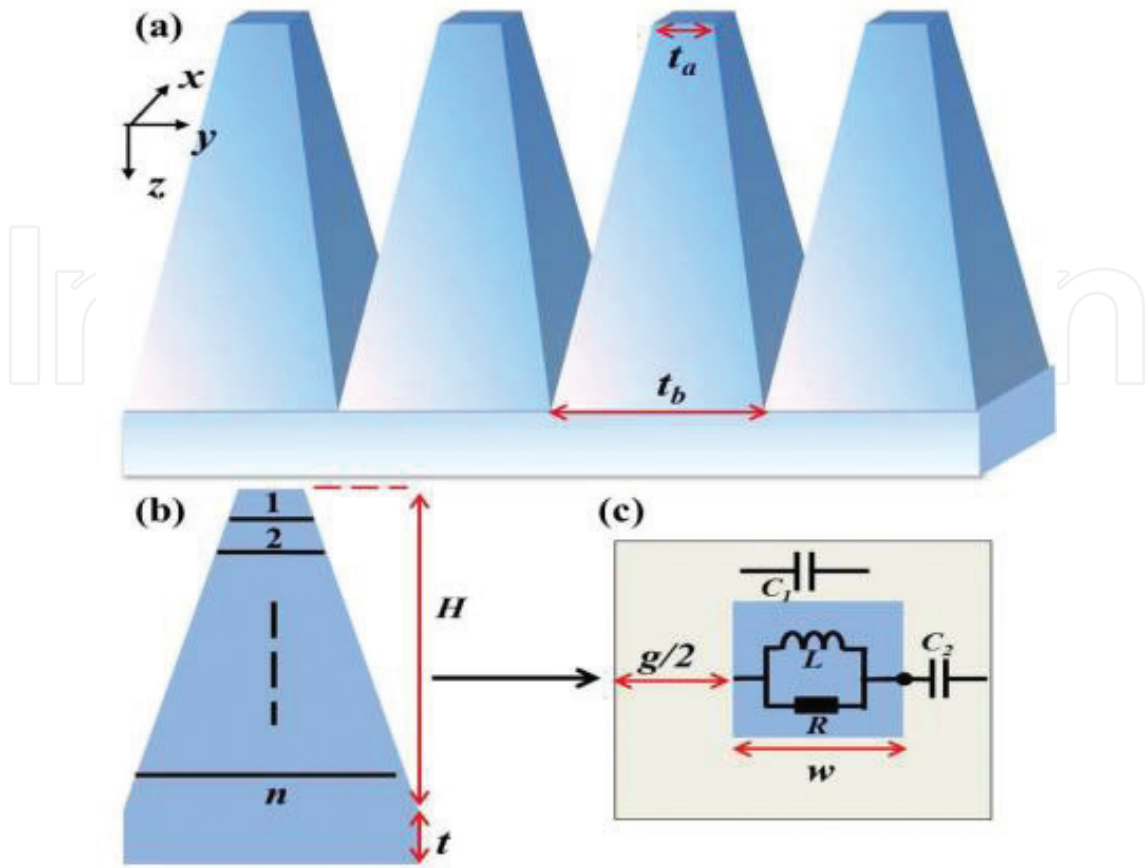
Figure 15. Schematic diagrams of (a) the super-flat absorber with atop span of t_a = 0.1 µm, bottom span of t_b = 1 µm, and ground plane thickness of t = 0.2 µm. (b) Side view of unit cell with H = 1.6 µm and (c) corresponding equivalent lumped circuit elements (adapted from Ref. [52], **Figure 1**).

The designed absorber unit consists of two TCOs elements (**Figure 15**): a truncated pyramid shaped resonator and a ground plane. The material used for the two elements can be only TCOs, i.e. materials for resonator and substrate are ITO. To establish the equivalent nanocircuit model for this absorber, one can hypothetically cut the whole pattern into n pieces along $k(z)$-direction (**Figure 15b**).

The first step is to extract the equivalent reactance of a single piece (same as those in Sections 3.1 and 3.2). The local impedances of ITO patch (Z_{ITO}), air gaps (Z_{c1}, Z_{c2}) and total effective impedance (Z_{eff}) can be calculated as,

$$Z_{ITO} = Z_R \| Z_L = i/\omega h \varepsilon_{ITO},$$
$$Z_{C_1} = iw/\omega h g \varepsilon_{air}, \quad Z_{C_2} = ig/\omega h(w+g)\varepsilon_{air}, \tag{26}$$
$$Z_{eff} = Z_{ITO} \| Z_{C_1} + Z_{C_2}, \quad Y = 1/Z_{eff}.$$

When taking the single piece into the transmission line (TL) model, it can be modelled as a shunt admittance Y (=$1/Z_{eff}$), and sandwiched between two semi-infinite transmission lines with characteristic impedance Z_0 (**Figure 16a**).
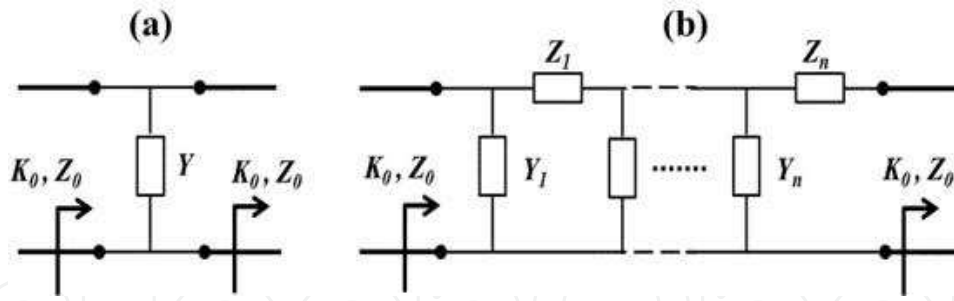
Figure 16. Transmission-line models of the truncated pyramid structure with (a) only a single piece and (b) a stack of n pieces (adapted from Ref. [52], **Figure 2**).

The second step is to connect each impedance into a complete TL circuit model. Series configuration of Z_i alongside with parallel configurations Y_i in layered stacked two-port networks, as shown in **Figure 16b**. The added series configuration Z_i is used to describe the conductive property between the adjacent pieces. For a thin uniform piece (P_i) of thickness l, the impedance Z_i can be approximately evaluated as $Z_i = 2(i\omega l p \mu_0/w_i)$ [54]. Note that in both scenarios, the realistic circuit value varies with the width of each P_i. The *ABCD*-matrix [55] for P_i of a lumped parallel electronic element combination with a series electronic element is

$$\begin{bmatrix} A_i & B_i \\ C_i & D_i \end{bmatrix} = \begin{bmatrix} 1 & 0 \\ Y_i & 1 \end{bmatrix} \begin{bmatrix} 1 & Z_i \\ 0 & 1 \end{bmatrix}. \tag{27}$$

For the whole structure with n pieces, it can be thought as an n-order filter along the transmission line, so the ABCD-matrix is expressed as,

$$\begin{bmatrix} A & B \\ C & D \end{bmatrix} = \begin{bmatrix} A_1 & B_1 \\ C_1 & D_1 \end{bmatrix} \cdots \begin{bmatrix} A_n & B_n \\ C_n & D_n \end{bmatrix}, \tag{28}$$

and the S matrix can be calculated as,

$$\begin{bmatrix} S_{11} & S_{12} \\ S_{21} & S_{22} \end{bmatrix} = \begin{bmatrix} \dfrac{AZ_0 + B - (CZ_0 + D)Z_0}{AZ_0 + B + (CZ_0 + D)Z_0} & \dfrac{2Z_0}{AZ_0 + B + (CZ_0 + D)Z_0} \\[2ex] \dfrac{2Z_0}{AZ_0 + B + (CZ_0 + D)Z_0} & \dfrac{-AZ_0 + B - (CZ_0 - D)Z_0}{AZ_0 + B + (CZ_0 + D)Z_0} \end{bmatrix}. \tag{29}$$

Obviously, the transmission, reflection and absorption can be obtained from the S matrix as,

$$T(\omega) = |S_{21}(\omega)|^2, \quad R(\omega) = |S_{11}(\omega)|^2,$$
$$A(\omega) = 1 - T(\omega) - R(\omega) \tag{30}$$

In optical metatronic circuit, in order to have a parallel element between the two ports, ideally one needs to have a constant electric field across the nanoelement. Thus, each piece should be a thin slab with sub-wavelength thickness in the z-direction. Considering the present design, for a truncated pyramid structure with height $H = 1.6$ μm sketched in **Figure 15**, one can choose

the thickness as 100 nm (cut number n =16) to get accurate results, smaller than wavelength (1–3 μm). By solving the transmission model in **Figure 16b**, the theoretical result is within a wavelength range of 1–3 μm (**Figure 17a**). It indicates that the absorption bandwidth becomes obviously wider and the efficiency is almost larger than 90%. The corresponding FDTD result (**Figure 17a**) indicates the feasibility of such a rigorous solution of TL model to describe the mechanism of this absorber. A good agreement between simulated and theoretical absorption at the wavelength larger than 1.5 μm, and only a slight deviation at the top absorption efficiency is observed. Furthermore, the simulation result shows that it has a flat response with absorption near unit between 1.4 and 2.6 μm.

Note that there is a slight deviation at the top absorption efficiency between simulation and theoretical prediction; we attribute this to the fact that there have deviations from extracted equivalent parameters. We employ the same full-wave FDTD simulations, only change is the structure from truncated pyramid to full pyramid, the truncated cone and the full cone, respectively. The four absorption spectra are compared in **Figure 17b**. We can see that the absorption bandwidth changes slightly indicating that the geometry dependence of the absorption is relatively weak. The bandwidth decreasing from pyramid to cone shape is due to the decrease of corresponding response area, when square changes to circle with the same width (diameter). It should be pointed out here that each geometric parameters used in **Figure 15** are not optimal. If we take the height, top width and bottom width altogether into account, much broader bandwidth could be expected.

Above all, under the guidance of nanocircuit theory, one can realize a broadband super-flat perfect infrared absorber in a single TCO material for its nice transmission and conductive properties. This simplified configuration without multi-layered design might releases the fabrication and design difficulties and exhibits great potentials in the applications of infrared
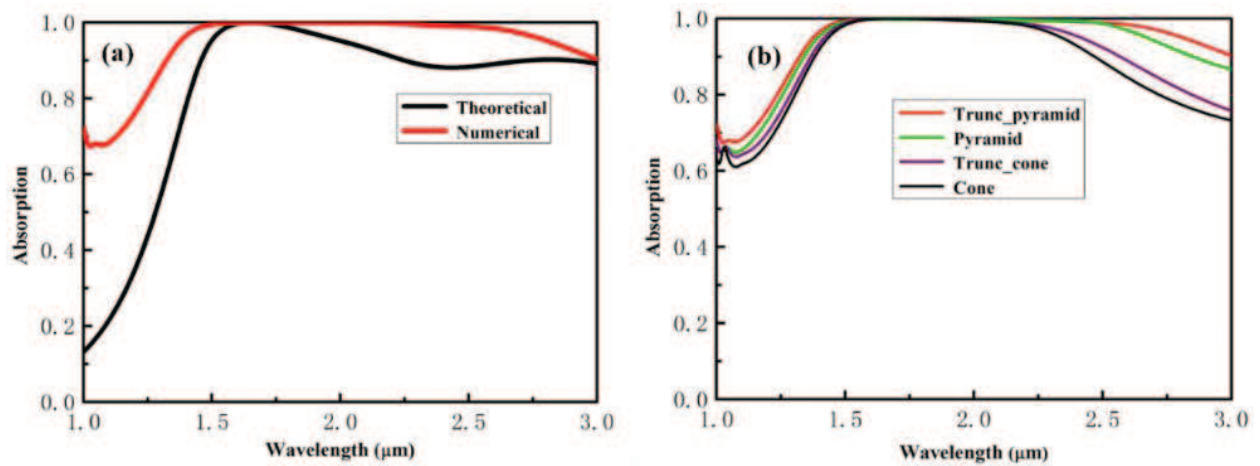
Figure 17. (a) Comparison between theoretical result from equivalent nanocircuit theory and numerical calculation from FDTD simulation. (b) Absorption curves under four different geometric structures. Truncated pyramid (t_a = 0.1 μm, t_b = 1 μm); pyramid (t_a = 0 μm, t_b = 1 μm); truncated cone (top diameter d_t = 0.1 μm, bottom diameter d_b = 1 μm); cone (top diameter d_t = 0 μm, bottom diameter d_b = 1 μm), H = 1.6 μm and t = 0.2 μm for the four structures (adapted from Ref. [52], **Figures 4** and **5**).

stealth system. Furthermore, this proposed equivalent circuit matrix algorithm is confirmed to be feasible enough to predict the complex frequency response of multi-layer nanostructures, and it can relieve the calculation from solving the multi-variable linear equations that can be easily extended to analyse other nanooptical devices.

4. Conclusions

In summary, thanks to the concept of metatronics, which gives us the possibility to transplant traditional circuit operations into a high-frequency nanodevice design. The equivalent nanocircuit (EN) theory is successfully confirmed to be feasible via the comparison with the numerical results from the rigorous FDTD calculation. With the toolbox of EN theory, an equivalent circuit matrix method can be used to conveniently predict the complicated frequency response of a complicated meta-material structure. Although here, only three application examples were demonstrated, it can be naturally and easily extended to analyse other nanooptical devices. Anyway, the interests in combining optical guiding devices with classical circuits is always high because the EN theory provides inspiring advances for designing more complex circuit systems and other related applied fields, although the deviation between results from EN theory and rigorous FDTD simulation indicates that the NE theory is still on the way of further perfection.

Acknowledgements

Author details

Qing Zhang[1,2], Jun You[3] and Chengpu Liu[1]*

*Address all correspondence to: chpliu@siom.ac.cn

1 State Key Laboratory of High Field Laser Physics, Shanghai Institute of Optics and Fine Mechanics, Chinese Academy of Sciences, Shanghai, China

2 Science and Technology on Plasma Physics Laboratory, Research Center of Laser Fusion, CAEP, Sichuan, China

3 Chinese Laser Press, Shanghai, China

References

[1] A. J. Holden, J. B. Pendry, W. J. Stewart, I. Youngs, Extremely low frequency plasmons in metallic mesostructures. *Physical Review Letters* **76**(25), 4773–4776 (1996).

[2] J. B. Pendry, A. J. Holden, D. J. Robbins, W. J. Stewart, Magnetism from conductors and enhanced nonlinear phenomena. *IEEE Transactions on Microwave Theory and Techniques* **47**, 2075–2084 (1999).

[3] J. B. Pendry, Negative refraction makes a perfect lens. *Physical Review Letters* **85**, 3966–3969 (2000).

[4] A. Alù, N. Engheta, All optical metamaterial circuit board at the nanoscale. *Physical Review Letters* **103**, 143902 (2009).

[5] A. Alù, M. E. Young, N. Engheta, Design of nanofilters for optical nanocircuits. *Physical Review B* **77**, 144107 (2008).

[6] N. Engheta, Circuits with light at nanoscales: Optical nanocircuits inspired by meta-materials. *Science* **317**, 1698–1702 (2007).

[7] Y. Sun, B. Edwards, A. Alù, N. Engheta, Experimental realization of optical lumped nanocircuits at infrared wavelengths. *Nature Materials* **11**, 208–212 (2012).

[8] N. Engheta, A. Salandrino, A. Alù, Circuit elements at optical frequencies: nanoinductors, nanocapacitors and nanoresistors. *Physical Review Letters* **95**, 095504 (2005).

[9] J. Jackson. Classical Electrodynamics. (Cambridge University Press, Cambridge, 1986).

[10] H. Caglayan, S.-H. Hong, B. Edwards, C. R. Kagan, N. Engheta, Near-infrared metatronic nanocircuits by design. *Physical Review Letters* **111**, 073904 (2013).

[11] A. Alù, N. Engheta, Input impedance, nanocircuit loading, and radiation tuning of optical nanoantennas. *Physical Review Letters* **101**, 043901 (2008).

[12] M. G. Silveirinha, A. Alù, J. Li, N. Engheta, Nanoinsulators and nanoconnectors for optical nanocircuits. *Journal of Applied Physics* **103**, 064305 (2008).

[13] N. Liu, F. Wen, Y. Zhao, Y. Wang, P. Nordlander, N. J. Halas, A. Alu`, Individual nano-antennas loaded with three-dimensional optical nanocircuits. *Nano Letters* **13**, 142–147 (2012).

[14] M. L. Brongersma, Plasmonics: Engineering optical nanoantennas. *Nature Photonics* **2**, 270–272 (2008).

[15] A. Alu, N. Engheta, Tuning the scattering response of optical nanoantennas with nano-circuit loads. *Nature Photonics* **2**, 307–310 (2008).

[16] F. Monticone, N. M. Estakhri, A. Alu, Full control of nanoscale optical transmission with a composite metascreen. *Physical Review Letters* **110**, 203903 (2013).

[17] M. Agio, A. Alù, *Optical antennas*. (Cambridge University Press, New York, 2013).

[18] C. L. Holloway, E. F. Kuester, J. A. Gordon, J. O'Hara, J. Booth, D. R. Smith, An overview of the theory and applications of metasurfaces: The two-dimensional equivalents of metamaterials. *IEEE Antennas and Propagation Magazine* **54**, 10–35 (2012).

[19] H. Cheng, S. Chen, P. Yu, W. Liu, Z. Li, J. Li, B. Xie, J. Tian, Dynamically tunable broadband infrared anomalous refraction based on graphene metasurfaces. *Advanced Optical Materials* **3**, 1744–1749 (2015).

[20] A. A. High, R. C. Devlin, A. Dibos, M. Polking, D. S. Wild, J. Perczel, N. P. de Leon, M. D. Lukin, H. Park, Visible-frequency hyperbolic metasurface. *Nature* **522**, 192–196 (2015).

[21] Z. Liu, Z. Li, Z. Liu, J. Li, H. Cheng, P. Yu, W. Liu, C. Tang, C. Gu, J. Li, High-performance broadband circularly polarized beam deflector by mirror effect of multinanorod metasurfaces. *Advanced Functional Materials* **25**, 5428–5434 (2015).

[22] X. Ni, N. K. Emani, A. V. Kildishev, A. Boltasseva, V. M. Shalaev, Broadband light bending with plasmonic nanoantennas. *Science* **335**, 427–427 (2012).

[23] S. Sun, Q. He, S. Xiao, Q. Xu, X. Li, L. Zhou, Gradient-index meta-surfaces as a bridge linking propagating waves and surface waves. *Nature Materials* **11**, 426–431 (2012).

[24] G. Zheng, H. Mühlenbernd, M. Kenney, G. Li, T. Zentgraf, S. Zhang, Metasurface holograms reaching 80% efficiency. *Nature Nanotechnology* **10**, 308–312 (2015).

[25] Y. Zhao, A. Alù, Manipulating light polarization with ultrathin plasmonic metasurfaces. *Physical Review B* **84**, 205428 (2011).

[26] A. Arbabi, Y. Horie, M. Bagheri, A. Faraon, Dielectric metasurfaces for complete control of phase and polarization with subwavelength spatial resolution and high transmission. *Nature Nanotechnology* **10**, 937–43 (2015).

[27] A. Arbabi, Y. Horie, A. J. Ball, M. Bagheri, A. Faraon, Subwavelength-thick lenses with high numerical apertures and large efficiency based on high-contrast transmitarrays. *Nature Communications* **6**, 7069 (2015).

[28] E. Arbabi, A. Arbabi, S. M. Kamali, Y. Horie, A. Faraon, Multiwavelength polarization-insensitive lenses based on dielectric metasurfaces with meta-molecules. *Optica* **3**, 628–633 (2016).

[29] S. M. Kamali, E. Arbabi, A. Arbabi, Y. Horie, A. Faraon, Highly tunable elastic dielectric metasurface lenses. *Laser & Photonics Reviews* **10**, 1062–1062 (2016).

[30] M. Al-Joumayly, N. Behdad, A new technique for design of low-profile, second-order, bandpass frequency selective surfaces. *IEEE Transactions on Antennas and Propagation* **57**, 452–459 (2009).

[31] K. Sarabandi, N. Behdad, A frequency selective surface with miniaturized elements. *IEEE Transactions on Antennas and Propagation* **55**, 1239–1245 (2007).

[32] Q. Zhang, L. Bai, Z. Bai, P. Hu, C. Liu, Equivalent-nanocircuit-theory-based design to infrared broad band-stop filters. *Optics Express* **23**, 8290–8297 (2015).

[33] H. S. Jeong, H.-J. Jeon, Y. H. Kim, M. B. Oh, P. Kumar, S.-W. Kang, H.-T. Jung, Bifunctional ITO layer with a high resolution, surface nano-pattern for alignment and switching of LCs in device applications. *NPG Asia Materials* **4**, e7 (2012).

[34] G. L. Matthaei, L. Young, E. Jones, *Microwave filters, impedance-matching networks, and coupling structures*. (Artech House, Norwood, Massachusetts, 1964).

[35] Q. Zhang, P. Hu, C. Liu, Giant-enhancement of extraordinary optical transmission through nanohole arrays blocked by plasmonic gold mushroom caps. *Optics Communications* **335**, 231–236 (2015).

[36] Q. Zhang, P. Hu, C. Liu, Realization of enhanced light directional beaming via a Bull's eye structure composed with circular disk and conical tip. *Optics Communications* **339**, 216–221 (2015).

[37] J.-X. Tan, Y.-B. Xie, J.-W. Dong, H.-Z. Wang, Flat-top transmission band in periodic plasmonic ring resonators. *Plasmonics* **7**, 435–439 (2012).

[38] C. Saeidi, D. van der Weide, Nanoparticle array based optical frequency selective surfaces: Theory and design. *Optics Express* **21**, 16170–16180 (2013).

[39] C. Saeidi, D. van der Weide, Synthesizing frequency selective metasurfaces with nanodisks. *Applied Physics Letters* **103**, 183101 (2013).

[40] M. Diem, T. Koschny, C. M. Soukoulis, Wide-angle perfect absorber/thermal emitter in the terahertz regime. *Physical Review B* **79**, 033101 (2009).

[41] X. Liu, T. Starr, A. F. Starr, W. J. Padilla, Infrared spatial and frequency selective metamaterial with near-unity absorbance. *Physical Review Letters* **104**, 207403 (2010).

[42] J. F. Federici, B. Schulkin, F. Huang, D. Gary, R. Barat, F. Oliveira, D. Zimdars, THz imaging and sensing for security applications—explosives, weapons and drugs. *Semiconductor Science and Technology* **20**, S266 (2005).

[43] J. B. Pendry, D. Schurig, D. R. Smith, Controlling electromagnetic fields. *Science* **312**, 1780–1782 (2006).

[44] N. Landy, S. Sajuyigbe, J. Mock, D. Smith, W. Padilla, Perfect metamaterial absorber. *Physical Review Letters* **100**, 207402 (2008).

[45] J. Hao, J. Wang, X. Liu, W. J. Padilla, L. Zhou, M. Qiu, High performance optical absorber based on a plasmonic metamaterial. *Applied Physics Letters* **96**, 251104 (2010).

[46] X. Liu, T. Tyler, T. Starr, A. F. Starr, N. M. Jokerst, W. J. Padilla, Taming the blackbody with infrared metamaterials as selective thermal emitters. *Physical Review Letters* **107**, 045901 (2011).

[47] J. Zhou, A. F. Kaplan, L. Chen, L. J. Guo, Experiment and theory of the broadband absorption by a tapered hyperbolic metamaterial array. *ACS Photonics* **1**, 618–624 (2014).

[48] F. Ding, Y. Cui, X. Ge, Y. Jin, S. He, Ultra-broadband microwave metamaterial absorber. *Applied Physics Letters* **100**, 103506 (2012).

[49] Q. Liang, T. Wang, Z. Lu, Q. Sun, Y. Fu, W. Yu, Metamaterial-based two dimensional plasmonic subwavelength structures offer the broadest waveband light harvesting. *Advanced Optical Materials* **1**, 43–49 (2013).

[50] Q. Zhang, L. Bai, Z. Bai, P. Hu, C. Liu, Theoretical analysis and design of a near-infrared broadband absorber based on EC model. *Optics Express* **23**, 8910–8917 (2015).

[51] N. Zhang, P. Zhou, L. Zhang, X. Weng, J. Xie, L. Deng, Ultra-broadband absorption in mid-infrared spectrum with graded permittivity metamaterial waveguide structure. *Applied Physics B* **118**, 409–415 (2015).

[52] Q. Zhang, L. Bai, X. Liu, C. Liu, X. Cui, Simplified transparent conductive Oxides-based ultrabroadband absorber design. *Journal of Lightwave Technology* **34**, 1354–1359 (2016).

[53] G. V. Naik, J. Kim, A. Boltasseva, Oxides and nitrides as alternative plasmonic materials in the optical range [Invited]. *Optical Materials Express* **1**, 1090–1099 (2011).

[54] F. Abbasi, N. Engheta, Roles of epsilon-near-zero (ENZ) and mu-near-zero (MNZ) materials in optical metatronic circuit networks. *Optics Express* **22**, 25109–25119 (2014).

[55] G. L. Matthaei, L. Young, E. M. T. Jones, *Microwave filters, impedance-matching networks, and coupling structures*. (Artech House, Dedham, Massachusetts, 1980).